Optics Letters

Single photon detection system for visible and infrared spectrum range

Alexander Divochiy,[1,2,†] Marta Misiaszek,[3,†,*] Yury Vakhtomin,[1,2] Pavel Morozov,[1,2] Konstantin Smirnov,[1,2,4] Philipp Zolotov,[1,2,4] and Piotr Kolenderski[3]

[1]LLC SCONTEL, 5/1-14 L'va Tolstogo st., Moscow 119021, Russia
[2]Moscow State University of Education, 1/1 M. Pirogovskaya st., Moscow 119991, Russia
[3]Faculty of Physics, Astronomy and Informatics, Nicolaus Copernicus University, Grudziadzka 5, 87-100 Torun, Poland
[4]National Research University Higher School of Economics, Moscow 101000, Russia
*Corresponding author: misiek@fizyka.umk.pl

Received 4 September 2018; revised 13 November 2018; accepted 14 November 2018; posted 15 November 2018 (Doc. ID 341001); published 14 December 2018

We demonstrate niobium nitride based superconducting single-photon detectors sensitive in the spectral range 452–2300 nm. The system performance was tested in a real-life experiment with correlated photons generated by means of spontaneous parametric downconversion, where one photon was in the visible range and the other was in the infrared range. We measured a signal to noise ratio as high as 4×10^4 in our detection setting. A photon detection efficiency as high as 64% at 1550 nm and 15% at 2300 nm was observed.

https://doi.org/10.1364/OL.43.006085

Recent advances in field of the superconducting single-photon detectors (SSPD) have introduced many conceptual ideas which allow us to progress their capabilities. Specifically, the quantum efficiency (QE) of SSPDs and the system detection efficiency (SDE) of SSPD-based systems have been increased to near-unity values at the telecom wavelength range [1–5]. The timing resolution can reach values below 17.8 ps [6], which are inaccessible for other single-photon detection technologies, such as silicon and InGaAs/InP photodiodes. In addition to that, SSPDs are considered to be the only available type of single-photon detectors capable of operation in the wide spectral range starting from near-UV [7] up to mid-IR [8–11] wavelengths. On the other hand, the small size of SSPDs makes it challenging to couple photons to their sensitive area. Typically, it requires single-mode fibers mounted directly to the SSPD.

As is known, the SDE of SSPDs depends on two quantities, the absorption and the intrinsic QR. The absorption depends on the properties of optical structures, incident field, and photon coupling with the sensitive area of a detector. The intrinsic QE is meant as the probability of resistive state formation due to an absorption event. It depends on the characteristics of the superconducting film. Both the parameters should be maximized in order to make SDE as high as possible. The former can be maximized by proper optical cavity fabrication and can reach near-unity values at a particular narrow wavelength range. On the other hand, the optimization of the intrinsic QE is a more complex task. It is higher at lower working temperature [8,11] and for narrow superconducting stripes [9], as for the materials with a lower superconductor energy gap of the superconducting material. However, the limits of the gap are dictated by the device operating temperature.

The very first implementation of SSPD with single-mode fluoride fiber input showed SDE below 1% at 2200 nm [12]. The detectors were cooled in liquid He_4 down to 1.7 K. More recently the use of multimode chalcogenide fiber (IRF-S-100) for transmission of mid-IR photons allowed detection of photons in the range up to 7 μm [10]. However, due to the mismatch in size between the fiber core and the detector, only 1% of the light incident on the fiber input reached the SSPD. As a material for fabrication of the superconducting structure, WSi was used. It has a lower critical temperature as compared to niobium nitride (NbN), so it can potentially be more useful for mid-IR applications. This is the price of having a working temperature in the sub-Kelvin range.

In this Letter, we show that the single-photon detecting system with NbN-based SSPDs, single-mode fibers, and a Gifford–McMahon cryocooler (Sumitomo RDK-101D) reaches characteristics which are superior to all previously published such systems for the wavelength range up to 2300 nm. In order to increase the intrinsic QE of the detectors, we used an approach similar to the one presented earlier [13], which allows us to fabricate disordered NbN films. In our previous work [14] we presented preliminary tests of detectors optimized for the 1600–2200 nm range. In addition, it was calculated that in the mid-IR wavelength region the intrinsic QE of the device could be as high as 10%. The presented coupling schemes could not find their place in the routine experiments because they imply significant prevalence of black body radiation over the signal of interest. To investigate exact values of the SDE of SSPD in the spectrum range up to 2300 nm, we suggest two main novelties with respect to the detector systems used in the telecom range. An optimized solution for the coupling scheme requires the use of SMF2000 single-mode fiber with the NbN devices. This significantly increases the allowed operation temperature of

the system, which is possible to reach in a typical close-cycle cryostat.

We used our standard technique [13,14] for fabrication of the devices analyzed here. The aim was to get higher absorption above 1550 nm, which was done by thickening the dielectric Si_3N_4 layer. This layer has a refractive index of 2.3 and a thickness of 185 nm. We begin with the analysis of the absorption of our devices as a function of incident photon wavelength.

We investigate the absorption for the spectral range of 800–2300 nm. It has been done in two steps by using two measurement apparatus depicted in Fig. 1: (a) the first for the range of 800–1700 nm and (b) the other one for the range of 1300–2300 nm.

For the analysis of the spectral absorption of our structures we used an optical spectrum analyzer (OSA) with built-in broadband radiation source allowing for measurement in the spectral rage of 800–1700 nm; see Fig. 1(a). We used a fiber splitter (FS; 50:50 distribution at 1550 nm) for simultaneous illumination and detection of the absorption and reference spectra. The broadband light source was connected to port number 1, and the OSA monitored the output port 2. Port number 3 was connected to either a gold mirror or the SSPD under the study. The reflected light was sent back and registered by the OSA. Port number 4 of the splitter was not used. The FS's partition coefficient is wavelength-dependent, and therefore, in order to perform absorption measurements of superconducting structures, the reference spectra with a gold mirror was acquired. We deposited a 100 nm thick gold layer on the standard ferrule to make sure that there was no air gap between the gold mirror and the fiber port 3. Thanks to that, in the scheme with the SSPD detector, we could calculate the absolute values of the absorption.

The measured spectra $P = P(\lambda)$ on port 2 of the fiber splitter, FS (see Fig. 1), in the case of SSPD and gold-tip fefrule, GF, are $P_{\mathrm{SSPD}}(\lambda) = T_{\mathrm{BS}}^2 R_{\mathrm{SSPD}} \cdot P_0(\lambda)$ and $P_{\mathrm{GF}}(\lambda) = T_{\mathrm{BS}}^2 R_{\mathrm{GF}} \cdot P(\lambda)$, respectively. Here $P(\lambda)$ is the light source spectrum, T_{BS} is the transmission coefficient of the FS, and R_{SSPD}, R_{GF} are the reflection coefficients of the superconducting structures and GF. Assuming perfect reflection from the gold mirror (GF), we can put $R_{\mathrm{GF}} = 1$. As a result, we get the relation $P_{\mathrm{SSPD}}/P_{\mathrm{GF}} = R_{\mathrm{SSPD}}$. By definition, the absorption coefficient reads $A_{\mathrm{SSPD}} = 1 - R_{\mathrm{SSPD}}$, so finally one gets $A_{\mathrm{SSPD}} = 1 - P_{\mathrm{SSPD}}/P_{\mathrm{GF}}$. The measured absorption is depicted in Fig. 2 with a blue curve.

In order to investigate SDE above 1700 nm, another measurement technique was developed. It is presented in Fig. 1(b).

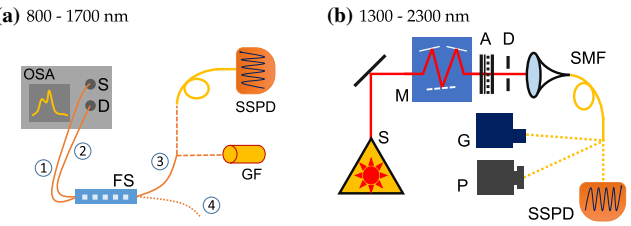

Fig. 1. Absorption measurement setups. For the range of (a) 800–1700 nm: OSA—optical spectrum analyzer (Keysight HP 70950A), S—radiation source, D—detector, FS—50:50 fiber splitter for 1550 nm, GF—gold-tip ferrule, SSPD—superconducting single-photon detector; (b) 1300–2300 nm: S—photon source (xenon lamp), M—monochromator, A—attenuator, D—diaphragm, detectors: G—Golay cell, P—power meter (Ophir PD-300 IRG), SSPD.

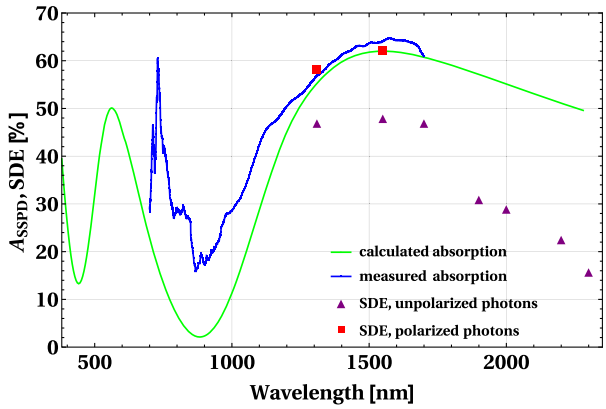

Fig. 2. Spectral absorption, A_{SSPD}, and system detection efficiency, SDE.

The experimental setup was based on an IR spectrophotometer (IKS-19). Light from the xenon lamp was led to the single diffraction grating with 300 grooves/mm. The output slit of 1 mm width defines a 5 nm bandwidth of the output radiation. Next, the radiation is attenuated by a set of Si wafers with deposited thin NbN films of thicknesses 5, 10, 20, and 30 nm and transmittances of 0.4, 0.1, 0.03, and 0.01, respectively. After the attenuator, we used a 0.5 mm diaphragm and the SM2000 single-mode fiber to collect free-space radiation.

Due to the fact that transmittance of attenuators depends on wavelength, we calibrated each of them on each the wavelength of interest by measuring power with and without attenuation. In order to measure power, we used a Golay cell (Tydex, GS-1D), which has 6 mm diameter input covered by a diamond window. Furthermore, it has noise equivalent power $\mathrm{NEP} = 10^{-9}\ \mathrm{W} \cdot \mathrm{Hz}^{-\frac{1}{2}}$, which does not vary in the spectral range of interest. As a result, it perfectly meets the requirements of our experiment. In order to use the Golay cell as a power meter, we measured its responsivity, which was estimated to be 6800 V/W. The responsivity measurement was performed using a 1550 nm diode laser and a power meter (Ophir, PD-300 IRG). In order to define the part of the optical power that can be collected to the single-mode fiber, we measured power at the fiber output directly with the power meter in the range of 1310–1600 nm. The power meter accuracy is 1 pW in this spectral range. By comparing these results with those achieved on the output of the monochromator with the Golay cell, we found that the coupling coefficient is equal to 0.0189(8). We assume this coefficient to be constant for the spectral range of 1310–2300 nm.

For the measurements, the target power of 0.5–2 pW was adjusted using a set of attenuators. Single mode fiber, SM2000, was connected to the optical input of the SSPD. The SDE was calculated by measuring the number of electrical pulses using a universal frequency counter (Agilent, A53131). The results of the experiment are presented in Fig. 2 with purple triangles. Note that the difference between the SDEs for polarized and unpolarized light stems from the meander-type geometry of the SSPD [15,16]. The system detection efficiency at 1310 and 1550 nm was approximately 0.45. Then efficiency decreases with decreasing photon energies. In order to estimate the maximal SDE values we also measured QE with a linearly

polarized light source at available wavelengths. In this case the best values for our detectors were 0.58 and 0.62 at 1310 and 1550 nm, respectively.

In our work spectral simulations of absorption for the range of 380–2300 nm were performed with OpenFilters software [17]. We adopted parameters of our sample from previous work [15]. Note that the optical properties of thin NbN films vary [15,18], which could be explained by differences in the stoichiometry of the films. The absorption coefficient was calculated for unpolarized radiation incident on a $Au/Si_3N_4/NbN$ structure (80/185/5 nm thick, respectively) from the SiO_2 medium. In our simulation we assume that the film is uniform, because the etched regions are much smaller than the wavelengths. The NbN meander pattern with filling factor of 0.5 is ignored. The green curve in Fig. 2 presents the simulated absorption spectral dependence for the superconducting structure. A fair agreement between the measured and simulated characteristics in the region of 1300–1700 nm confirms the accuracy of our backreflection method, which justifies its application for future spectral data analysis.

Finally, we tested our SSPDs with a correlated photon source based on the process of spontaneous parametric down-conversion, which we use to investigate their performance in correlation-type measurements[19,20]. The experimental setup is depicted in Fig. 3. A frequency doubled tunable Ti:sapphire laser pumps the photon pair source based on a periodically poled potassium titanyl phosphate (PPKTP) crystal. The photons are coupled into single mode fibers. The spectra of the output photons can be modified by tuning the pump photon spectrum. The pump beam is tuned in the range of 377–404 nm. It allows for generation of pairs of photons, where one photon is in the 452–575 nm spectral range and the other one in the 1363–2299 range. The measured tuning curve is presented in Fig. 4. The pump and visible photon spectra are analyzed using a spectrometer. The spectrum of the infrared photon is calculated based on the energy conservation relation.

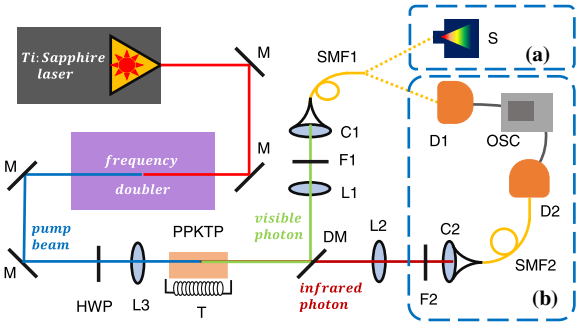

Fig. 3. Experimental setup. Pulsed Ti:sapphire laser, M—mirror, L3—lens (focal lengh $f = 10$ cm), PPKTP—periodically poled potassium titanyl phosphate crystal, T—temperature controller, DM—dichroic mirror (Semrock 76-875 LP), L1, L2—plano–convex lens ($f = 12$ cm, 15 cm), F1—set of filters [three settings: (1) Chroma ET500 and Z532-rdc, (2) 2 pcs of AHF 442 LP, (3) 2pcs of AHF 442 LP and Thorlabs FESH0700], C1, C2—single-mode fiber coupler ($f = 0.8$ cm, 1.51 cm), F2—long-pass filter (Semrock BLP01-1319R), SMF1, SMF2—single mode fiber [two settings: (1) Thorlabs SMF460B and SMF1550, (2) SMF780 and SMF2000]. Detection setups: (a) S—spectrometer (Ocean Optics USB2000+); (b) D1, D2—detectors, OSC—oscilloscope.

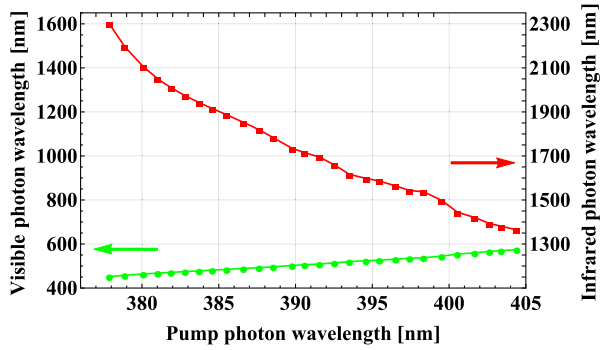

Fig. 4. Generated photon wavelengths. Green dots show measured wavelengths of the visible photon, and red ones are calculated from the energy conservation relation.

The coincidence measurements are performed using three types of detectors: (1) SSPD: bias current 21 μA; (2) InGaAs/InP, detection efficiency 10%, gate width 20 ns, dead-time 10 μs; and (3) silicon avalanche photodiode (Si APD). The output signals from the detectors are then analyzed using an oscilloscope, Fig. 3(b). The timing histogram of the relative pulse arrival times are measured. The data set consists of 10^4 samples. Figure 5(a) shows examples of measurement results for

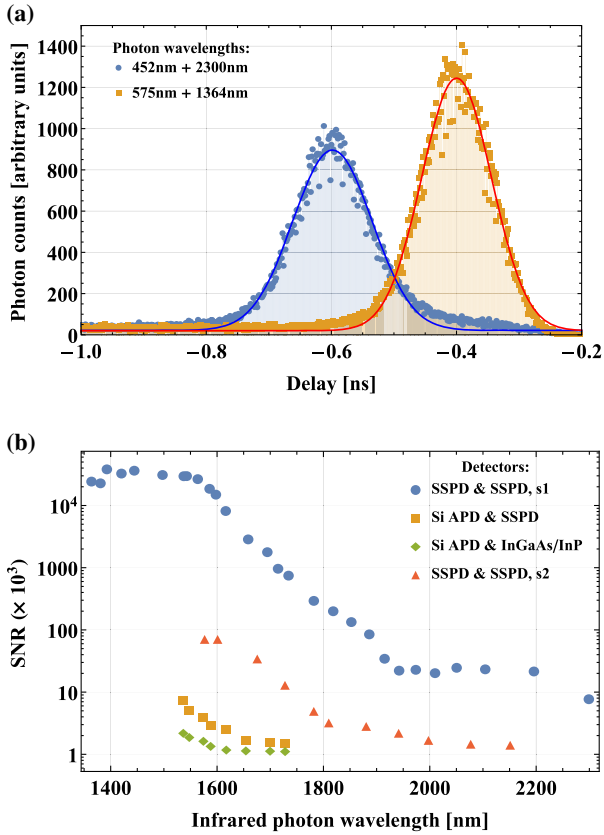

Fig. 5. (a) Arrival time coincidence histograms for two example settings. The measured setup timing jitter is approximately 86 ps (FWHM). (b) SNR for four different settings as described in the main text. Plot markers are bigger than error bars, excluding SNR values close to 1.

different pairs of detectors: (a) Si APD and InGaAs/InP, (b) Si APD and SSPD, and (c) two SSPDs.

The coincidence counting measurement results, as seen in Fig. 5(a), allow us to estimate the signal to noise ratio (SNR) by fitting the Gaussian function $b + a\ \exp[-4\ \ln\ 2(t - t_0)^2/\sigma^2]$ to the timing histograms. In our model b stands for the background noise, a is the signal amplitude, σ is the timing jitter, and t_0 is the time where the peak maximum value occurs. Based on this definition SNR $= a/b\sqrt{\pi/16\ \log(2)}\mathrm{erf}(2\sqrt{\log(2)}) \approx 0.52a/b$.

The SNR results are gathered in panel (b) in Fig. 5. We compare SSPDs with InGaAs/InP detectors in exactly the same settings (F1 filter setting 1 and fibers setting 1 as described in caption of Fig. 3). The results are depicted with green diamonds and orange squares. One can clearly see the limit around 1650 nm beyond which the InGaAs/InP detector QE drops to zero. The dark count rate of our Si APD was around 3 kcps, which originated in an intrinsic dark count of the detector itself and stray light. The typical Si APDs' noise is around 100 cps. Therefore, in principle, it is expected that SNR can increase in that case by one order of magnitude. Moreover, one can observe a plateau in the range 1900–2200 nm, which we attribute to the interplay of SDE for visible and infrared photons.

Next, we use two SSPD detectors with different filters (F1 filter as denoted in setting 2 in Fig. 3). The measurement results are marked using red triangles. This filter allows us to investigate the system performance in the broad range of wavelengths up to 2151 nm. One can also see the improved SNR by approximately one order of magnitude. In the following step the SNR was improved by approximately two orders of magnitude by replacing the fibers (setting 2) and filters (setting 3). This allowed us to broaden the spectral range even further. It should be noted that in the range 1900–2300 nm the SSPDs efficiency drop can be explained by small photon energies.

Recently, in [5] we experimentally showed that the fabrication of SSPD detectors based on structurally disordered films [21–24] allows for saturated dependence of the detection efficiency at lower bias current. This is based on the observation that the critical temperature and the electron diffusion coefficient follow the trend of the Ioffe–Regel parameter [25], which is a measure of the degree of disorder. Therefore this mechanism has the potential to increase the internal photon detection efficiency of an SSPD for the infrared photon wavelength range.

Summarizing, we have developed the principles of the realization of the single photon receivers above the telecom wavelength range based on NbN SSPD with high values of system detection efficiency. It was achieved by using more disordered NbN films. The best values of the system detection efficiency are 60% at 1700 nm, 25% at 2000 nm, and 15% at 2300 nm. Within the experimental scenario involving the entangled photons we have compared our SSPDs with other detectors. The best performance was achieved when using an SSPD/SSPD pair, which yielded at least three orders of magnitude better SNR as compared to the others. In this case the achieved values of the SNR were >20000 up to 1600 nm, >1000 in the wavelength range 1600–1700 nm, >100 for 1700–1850 nm, and >8 at around a 1850–2300 nm.

Funding. Fundacja na rzecz Nauki Polskiej (FNP) (project First Team/2017-3/20) cofinanced by the European Union under the European Regional Development Fund (ERDF); Ministerstwo Nauki i Szkolnictwa Wyższego (MNiSW) (6576/IA/SP/2016); Narodowe Centrum Nauki (NCN) (2016/23/D/ST2/02064, Sonata 12); Russian Science Foundation (RSF) (18-12-00364).

[†]These authors contributed equally to this work.

REFERENCES

1. F. Marsili, V. B. Verma, J. A. Stern, S. Harrington, A. E. Lita, T. Gerrits, I. Vayshenker, B. Baek, M. D. Shaw, R. P. Mirin, and S. W. Nam, Nat. Photonics **7**, 210 (2013).
2. V. B. Verma, B. Korzh, F. Bussières, R. D. Horansky, S. D. Dyer, A. E. Lita, I. Vayshenker, F. Marsili, M. D. Shaw, H. Zbinden, R. P. Mirin, and S. W. Nam, Opt. Express **23**, 33792 (2015).
3. I. Esmaeil Zadeh, J. W. Los, R. B. Gourgues, V. Steinmetz, G. Bulgarini, S. M. Dobrovolskiy, V. Zwiller, and S. N. Dorenbos, APL Photon. **2**, 111301 (2017).
4. W. Zhang, L. You, H. Li, J. Huang, C. Lv, L. Zhang, X. Liu, J. Wu, Z. Wang, and X. Xie, Sci. China: Phys., Mech. Astron. **60**, 120314 (2017).
5. K. Smirnov, A. Divochiy, Y. Vakhtomin, P. Morozov, P. Zolotov, A. Antipov, and V. Seleznev, Supercond. Sci. Technol. **31**, 035011 (2018).
6. V. Shcheslavskiy, P. Morozov, A. Divochiy, Y. Vakhtomin, K. Smirnov, and W. Becker, Rev. Sci. Instrum. **87**, 053117 (2016).
7. E. E. Wollman, V. B. Verma, A. D. Beyer, R. M. Briggs, B. Korzh, J. P. Allmaras, F. Marsili, A. E. Lita, R. P. Mirin, S. W. Nam, and M. D. Shaw, Opt. Express **25**, 26792 (2017).
8. G. Gol'tsman, O. Minaeva, A. Korneev, M. Tarkhov, I. Rubtsova, A. Divochiy, I. Milostnaya, G. Chulkova, N. Kaurova, B. Voronov, D. Pan, J. Kitaygorsky, A. Cross, A. Pearlman, I. Komissarov, W. Slysz, M. Wegrzecki, P. Grabiec, and R. Sobolewski, IEEE Trans. Appl. Superconduct. **17**, 246 (2007).
9. F. Marsili, F. Bellei, F. Najafi, A. E. Dane, E. A. Dauler, R. J. Molnar, and K. K. Berggren, Nano Lett. **12**, 4799 (2012).
10. L. Chen, D. Schwarzer, V. B. Verma, M. J. Stevens, F. Marsili, R. P. Mirin, S. W. Nam, and A. M. Wodtke, Acc. Chem. Res. **50**, 1400 (2017).
11. F. Marsili, V. Verma, M. J. Stevens, J. A. Stern, M. D. Shaw, A. Miller, D. Schwarzer, A. Wodtke, R. P. Mirin, and S. W. Nam, *CLEO: Science and Innovations* (Optical Society of America, 2013), p. CTu1H.1.
12. D. Elvira, A. Michon, B. Fain, G. Patriarche, G. Beaudoin, I. Robert-Philip, Y. Vachtomin, A. V. Divochiy, K. V. Smirnov, G. N. Gol'tsman, I. Sagnes, and A. Beveratos, Appl. Phys. Lett. **97**, 131907 (2010).
13. K. Smirnov, A. Divochiy, Y. Vakhtomin, P. Morozov, P. Zolotov, A. Antipov, and V. Seleznev, Supercond. Sci. Technol. **31**, 035011 (2018).
14. P. I. Zolotov, A. V. Divochiy, Y. B. Vakhtomin, P. V. Morozov, V. A. Seleznev, and K. V. Smirnov, J. Phys. Conf. Ser. **917**, 062037 (2017).
15. V. Anant, A. J. Kerman, E. A. Dauler, J. K. Yang, K. M. Rosfjord, and K. K. Berggren, Opt. Express **16**, 10750 (2008).
16. S. N. Dorenbos, E. M. Reiger, N. Akopian, U. Perinetti, V. Zwiller, T. Zijlstra, and T. M. Klapwijk, Appl. Phys. Lett. **93**, 161102 (2008).
17. S. Larouche and L. Martinu, Appl. Opt. **47**, C219 (2008).
18. A. Semenov, B. Günther, U. Böttger, H.-W. Hübers, H. Bartolf, A. Engel, A. Schilling, K. Ilin, M. Siegel, R. Schneider, D. Gerthsen, and N. A. Gippius, Phys. Rev. B **80**, 054510 (2009).
19. T. Lutz, P. Kolenderski, and T. Jennewein, Opt. Lett. **39**, 1481 (2014).
20. M. Misiaszek, A. Gajewski, and P. Kolenderski, J. Phys. Commun. **2**, 065014 (2018).
21. T. I. Baturina, A. Y. Mironov, V. M. Vinokur, M. R. Baklanov, and C. Strunk, Phys. Rev. Lett. **99**, 257003 (2007).
22. V. Gantmakher and V. T. Dolgopolov, Phys. Usp. **53**, 1 (2010).
23. S. P. Chockalingam, M. Chand, J. Jesudasan, V. Tripathi, and P. Raychaudhuri, Phys. Rev. B **77**, 214503 (2008).
24. S. P. Chockalingam, M. Chand, A. Kamlapure, J. Jesudasan, A. Mishra, V. Tripathi, and P. Raychaudhuri, Phys. Rev. B **79**, 094509 (2009).
25. D. Y. Vodolazov, Phys. Rev. Appl. **7**, 034014 (2017).